Solvent Synthesis, Growth Mechanism and Photocatalytic Properties of $AgInS_2$ Nanoplate and Nanoparticle

WANG Yue[1](王　跃);SHI Yong-Fang[2] (石永芳);LI Xiao-Bo[1] (李晓波);LI Dong-Wei[1] (黎东维);ZHANG Tao[1] (张涛);HE Yu-Cen[1] (何昱岑)

[1]*College of Biological and Chemical Engineering, Chongqing University of Education, Chongqing* 400067, *China*;[2]*Fujian Institute of Research on the Structure of Matter, Key Laboratory of Research on Chemistry and Physics of Optoelectronic Materials*, *Chinese Academy of Sciences, Fuzhou* 350002, *China*

ABSTRACT Orthorhombic $AgInS_2$ nanoplate and nanoparticle were synthesized using pyridine and 1-dodecanethiol as the solvent. The obtained products were characterized by X-ray diffraction (XRD), field-emission scanning electron microscope (FESEM), field-emission transmission electron microscope (FETEM), and the possible growth mechanism of $AgInS_2$ was also proposed by the exploration of reaction temperature and time. Meanwhile, the bandgap of $AgInS_2$ was calculated by the UV-Vis diffuse reflectance spectrum, and the photocatalytic activity was also investigated. Those experimental results indicate that the reaction temperature, reaction time and solvent have an influence on phase and morphology of $AgInS_2$, and both $AgInS_2$ nanoplate and nanoparticle have some ability on photocatalytic degradation of organic dyes under UV-Vis light irradiation.

Keywords: **orthorhombic $AgInS_2$; nanostructure; solvent method; growth mechanism; photocatalysis;**

DOI: 10.14102/j.cnki.0254-5861.2011-1738

1 INTRODUCTION

With the development of society, people pay more and more attention to the pollution caused by industrial waste water[1]. The semiconductor photocatalytic method, especially using cheap sunlight as the light source, to realize visible photocatalytic degradation of pollutants is a new technology of low energy consumption and environmental protection. As an important I-II-VI group semiconductor material, ternary metal sulfide, $AgInS_2$, has gradually become a research hotspot, due to its unique photoelectric and catalytic performance, which has potential application prospect in the fields of light-emitting diodes, nonlinear optical

devices, solar cells, photocatalysis and biological labeling[2-9]. Currently, the preparation methods of $AgInS_2$ are hot pressing method[10], hot-wall epitaxial growth method[11], hydrothermal method[12], solvothermal method[13], hot injection method[14], thermolysis method[15], *etc*. The previous work focuses on the 0D $AgInS_2$ quantum dots[8, 9], but few studies of 2D and 3D nanostructures[4]. In our previous work[16], the metastable orthorhombic $AgInS_2$ flower-like microsphere was successfully prepared by the pyrolysis of organometallic precursors at 250～280 ℃. However, considering the high temperature (above 200 ℃) needs high energy consumption, and the products should be heated more uniformly in the solvent, as well as the solvent has important influence on the morphology of the product, we try to disperse the precursor in different solvents to obtain $AgInS_2$ nanostructures with different morphology at lower temperature. The results indicate that $AgInS_2$ nanoplate and nanoparticle can be obtained at lower temperature (120～150 ℃) using pyridine and 1-dodecanethiol as the solvents. Meanwhile, the obtained products were characterized by X-ray diffraction (XRD), field-emission scanning electron microscope (FESEM) and field-emission transmission electron microscope (FETEM), and the possible growth mechanism of $AgInS_2$ was also proposed by the exploration of reaction temperature and time. Finally, the bandgap of $AgInS_2$ was calculated by UV-Vis diffuse reflectance spectrum, and the photocatalytic activity was also investigated, as well as its possible photocatalytic mechanism.

2 EXPERIMENTAL

2. 1 Chemicals

Silver nitrate ($AgNO_3$), indium nitrate hydrate ($In(NO_3)_3 \cdot 4.5H_2O$), carbon disulfide (CS_2), potassium hydrate (KOH), ethanol (C_2H_5OH), chloroform ($CHCl_3$), dichloromethane (CH_2Cl_2), and pyridine (C_5H_5N), dichloromethane (CH_2Cl_2), 1-dodecanethiol ($C_{12}H_{25}SH$), ethylenediamine ($C_2H_8N_2$), and oleic acid ($C_{18}H_{34}O_2$) were purchased from Shanghai Chemical Co.. $[CH_3(CH_2)_7]_2NH$ (Alfa, A.R.) was used. All reactants were used as received.

2. 2 Syntheses of Ag(OTC) and $In(OTC)_3$ precursors

Precursors were prepared according to the reactions shown in Scheme 1. Below 0 ℃, CS_2 has reacted with $[CH_3(CH_2)_7]_2NH$ and KOH to produce enough dithiocarbamate salt in ethanol (Reaction 1). Then, an ethanol solution with excess $In(NO_3)_3 \cdot 4.5H_2O$ was added to generate white suspension $In[S_2CN(C_8H_{17})_2]_3$ (Reaction 2). After stirring for 5 min, an ethanol solution with an appropriate amount of $AgNO_3$ with a mole ratio of M^+:In^{3+}

= 1:1.25 was added and stirred for another 2 h to ensure the complete reaction to form $In(OTC)_3$ and Ag(OTC) precursors (Reaction 3) and make them mix evenly. A solid was obtained after rotary evaporation of ethanol and then dissolved in $CHCl_3$ and filtrated. Then, this $CHCl_3$-filtration was rotary evaporated to generate the Ag(OTC)/$In(OTC)_3$ precursor, a soil-like solid. Finally, the precursors in yellow were washed by acetone.

2. 3 Synthesis of $AgInS_2$

In a typical process, the precursor was added into a solution containing pyridine or other solvents. The mixture was stirred for 15 min at room temperature in air, and then poured into a 25 mL Teflon-lined stainless autoclave. The autoclave was heated at 120～150 ℃ for 17.5～20 h under autogenous pressure, and then air-cooled to room temperature. The resulting precipitates were collected and washed with CH_2Cl_2 and ethanol thoroughly and dried at room temperature in air. The $AgInS_2$ product is dark red.

2. 4 Characterization

X-ray powder diffraction (XRD), transmission electron microscopy (TEM), high-resolution TEM (HRTEM), and scanning electron microscopy (SEM) were used to characterize the structure, composition, size, and shape of the synthesized nanoproducts, respectively. The XRD patterns were collected with the aid of a PANalytical X'Pert Pro diffractometer at room temperature at 40 kV and 40 mA (Cu$K\alpha$ radiation). The TEM images were obtained using a JEM 2010 TEM equipped with a field emission gun operating at 200 kV. Images were acquired digitally using a Gatan multipole scanning CCD camera with an imaging software system. The EDX analyses were performed on a carbon-film-coated Cu grid with the aid of a JEM 2010 TEM equipped with an Oxford INCA spectrometer. The optical diffuse reflectance spectrum was measured at room temperature using a Perkin-Elmer Lambda 900 UV-Vis spectrophotometer equipped with an integrating sphere attachment and $BaSO_4$ as reference. The UV-Vis spectra were measured on a Perkin-Elmer Lambda-35 spectrophotometer.

2. 5 Photocatalytic activity test

The photocatalytic activities of the samples were investigated by the decomposition rate of methyl orange (MO) or Methylene blue (MB) in an aqueous solution under UV-vis light irradiation. Briefly, 100 mg of $AgInS_2$ nanopowders was dispersed in 100 mL of MO or MB solution with an initial concentration of 10 ppm. Prior to irradiation, the suspension was stirred in the dark for 1 h to ensure the establishment of the adsorption-desorption equilibrium. The assembly was continuously stirred and irradiated by a 300 W halogen-tungsten lamp. At an irradiation time interval of 1 h, 4 mL of the suspension was collected and then the slurry samples including the photocatalyst and MO or MB solution were centrifuged to remove the photocatalyst particles. The concentration of MO or MB was analyzed by measuring the absorbance at 664 nm

wavelength for MB (or 463 nm wavelength for MO) using a UV-Vis spectrophotometer.

3 RESULTS AND DISCUSSION

3. 1 Phase and microstructure

The XRD patterns of the as-synthesized products prepared using pyridine as the solvent at 120 ℃ for 20 h (Fig. 1a) and using 1-dodecanethiol as the solvent at 150 ℃ for 17.5 h (Fig. 1b) can be indexed to the ICDD pattern (PDF#25-1328). We can see that the positions of all diffraction peaks correspond to (120), (002), (121), (202), (320), (123) and (322) planes and are in agreement with the orthorhombic phase of $AgInS_2$. From Fig. 1a and 1b, we can see two obvious differences between those patterns. One is the intensity of (002) plane at 26.6 ° in Fig. 1a whcih is much higher than that in Fig. 1b, indicating that the growth of nanosheets has a certain crystallographic orientation; the other is the peak width of (123) plane at 48.1 °in Fig. 1a which is much narrower than the one in Fig. 1b, probably due to the smaller size of nanoparticles. Furthermore, all the peaks in Fig. 1a are sharper than those in Fig. 1b correspondly, showing the nanoplates have better crystallinity.

As shown in Fig. 2a and 2b, the $AgInS_2$ produced in pyridine at 120 ℃ for 20 h is nanoplates with the width of 300～500 nm and thickness of about 40 nm, which are stacked and not well dispersed. However, $AgInS_2$ produced in 1-dodecanethiol at 150 ℃ for 17.5 h is irregular nanoparticles, which is severely agglomerated (SEM: Fig. 2c). Furthermore, from Fig. 2d we can see that the size of those nanoparticles should be less than 20 nm, and the dispersity is still not good even after ultrasonic concussion. Compared with the 0D nanoparticle, the 2D nanoplate takes a preferred orientation for powder diffraction, so the intensity of (002) diffraction peak is greatly increased, which also explains why the peak in Fig. 1a is significantly higher than that in Fig. 1b. A typical HRTEM image of the edge of such a nanoparticle with the size of about 14 nm (calculated by the red circle) is shown in Fig. 2e, further indicating the size of those particles is less than 20 nm. Clear lattice fringes (Fig. 2f) can be observed after FFT inversion and the single-crystal natures of the nanoparticles are revealed. The interplanar spacing is about 0.357 nm, in good agreement with the distance (0.356 nm) of (120) plane of the orthorhombic $AgInS_2$[17].

3. 2 Possible formation mechanism of $AgInS_2$

Using pyridine as the solvent, we can observe the formation of orthorhombic $AgInS_2$ by adjusting the reaction time under the condition of 120 ℃. When the reaction time was 5 h, a small amount of Ag_2S (Fig. 3a) with weak diffraction peak of XRD was obtained, and there were only two obvious peaks; when the reaction

time was increased to 10 h, the peak intensity of XRD (Fig. 3b) had been significantly enhanced, in good agreement with that of monoclinic Ag_2S (ICDD PDF# 14-0072). It can be seen from Fig. 3d that the Ag_2S also contains two morphologies, namely, the hexagon with a length of about 100 nm and the particle with size of about 50 nm, and the amount of particles is significantly more than the hexagon. When the reaction time was further extended to 15 h, the obvious diffraction peak of orthorhombic $AgInS_2$ appeared (Fig. 3c), and its intensity is higher than that of Ag_2S, indicating that most Ag_2S has been transformed into $AgInS_2$. Furthermore, the amount of original small particles greatly reduced, but both the number and size of the hexagonal sheet increased (Fig. 3e). This result shows that, as the reaction time is increased, the newly generated monoclinic Ag_2S gradually transforms into orthorhombic $AgInS_2$, accompanied by the transformation from particles to hexagonal plate. This point can be verified that pure orthorhombic $AgInS_2$ nanoplates are obtained when the reaction time is extended to 20 h (Fig. 1a and 2a).

According to the above experimental facts, combined with the previous work[18] and results obtained by our group[19, 20], we have proposed the possible growth mechanism of orthorhombic $AgInS_2$, and the reactions are as follows (HNR_2, R = $-C_8H_{17}$):

$$HNR_2 + KOH + CS_2 \longrightarrow KS_2CNR_2 + H_2O \qquad (1)$$

$$KS_2CNR_2 + AgNO_3 \longrightarrow AgS_2CNR_2 + KNO_3 \qquad (2)$$

$$KS_2CNR_2 + In(NO_3)_3 \longrightarrow In(S_2CNR_2)_3 + KNO_3 \qquad (3)$$

$$AgS_2CNR_2 \longrightarrow Ag_2S + \text{others} \qquad (4)$$

$$Ag_2S + In(S_2CNR_2)_3 \longrightarrow AgInS_2 + \text{others} \qquad (5)$$

Scheme 1. Reactions to generate $AgInS_2$

The as-prepared KS_2CNR_2 (Reaction 1) was coordinated with Ag^+ and In^{3+} to form the corresponding complex AgS_2CNR_2 (Reaction 2) and In $(S_2CNR_2)_3$ (Reaction 3). Since these complexes were formed in solution and have been fully stirred, it should not be a simple mechanical mixture in the final solid form, but rather a uniform mixture at the molecular level. As the reaction temperature increased, AgS_2CNR_2 began to decompose into corresponding Ag_2S (Reaction 4), because Ag^+ has a high diffusivity under high temperature, which can move freely in the lattice of cation hole[21]. Therefore, In^{3+}, released slowly from $In(S_2CNR_2)_3$, can replace part of Ag^+ in the Ag_2S lattice, forming orthorhombic $AgInS_2$ gradually (Reaction 5). On the other hand, when using pyridine as the solvent, the as-prepared Ag_2S particles wrapped by pyridine would grow anisotropically into lamellar structure; while using 1-dodecanethiol as the solvent the as-prepared Ag_2S particles wrapped by 1-dodecanethiol would grow isotropically into irregular particle with small size. Hence,

when the In^{3+} partially replaces Ag^{+} in the Ag_2S lattice, it will not change the morphology and finally the product grows into the nanoplates or nanoparticles, respectively.

3. 3 Effect of reaction temperature

In order to investigate the morphology-reaction temperature relationship, a batch of parallel reactions using pyridine as the solvent has been carried out, and some representative SEM images are displayed in Fig. 5. The detailed experimental results are listed in Table 1. The results indicated that when temperature is increased to 150 ℃, the products are also pure orthorhombic $AgInS_2$ nanoplate (XRD: Fig. 4a, SEM: Fig. 5a), similar to that of 120 ℃; while at 170 ℃, besides of orthorhombic $AgInS_2$, minor tetragonal $AgInS_2$ (ICDD PDF# 25-1330) begins to appear, and lots of nanopaticles are observed (XRD: Fig. 4b, SEM: Fig. 5b), indicating that some orthorhombic $AgInS_2$ have transformed into tetragonal $AgInS_2$, namely metastable phase transformes into stable phase[22], so the morphology of products takes an obvious change. When the temperature continues to rise to 190 ℃, the relative intensity of the diffraction peak of tetragonal phase is not significantly improved (Fig 4c), showing that the percentage of tetragonal phase has not significantly enhanced. The products are also nanoparticles similar to that of 170 ℃, but almost none of nanoplate is observed (Fig. 5c).

Therefore, using pyridine as the solvent, the optimal temperature range to synthesize orthorhombic $AgInS_2$ nanoplate is 120～150 ℃, and the optimal range of reaction time is 17.5～20 h. If the temperature is too low or the time is too short, the samples should not fully react to produce pure ternary sulfide $AgInS_2$. However, the higher temperature will make metastable $AgInS_2$ transform into tetragonal $AgInS_2$. It is interesting to find that when 1-dodecanethiol is used as the solvent, the orthorhombic $AgInS_2$ can be obtained at 120～190 ℃ for 17.5～20 h, which indicates that the solvent also plays a certain role in the formation of $AgInS_2$.

Table 1. Products Synthesized Using Pyridine as the Solvent at Different Temperature

Temperature (℃)	Time (h)	XRD	Phase	SEM	Morphology
150	17.5	Fig. 4a	Orthorhombic $AgInS_2$	Fig. 5a	Nanoplate
170	17.5	Fig. 4b	Orthorhombic $AgInS_2$ + tetragonal $AgInS_2$ (minor)	Fig. 5b	Nanoplate (minor) + nanoparticle
190	17.5	Fig. 4c	Orthorhombic $AgInS_2$ + tetragonal $AgInS_2$ (minor)	Fig. 5c	Nanoparticle

3. 4 Effect of the solvent

To further understand the effect of solvent, some other solvents are used instead of pyridine and 1-dodecanethiol. All these parallel reactions have been run at 150 ℃ for 17.5 h. The detailed experimental

results are listed in Table 2. When using ethylenediamine as the solvent, the product is a mixture containing lots of orthorhombic $AgInS_2$ and a small amount of tetragonal $AgInS_2$ (XRD: Fig. 6a); besides a small number of particles, most of products are square sheet with the thickness of 30～60 nm (SEM: 6c). While using oleic acid as the solvent, both orthorhombic $AgInS_2$ and monoclinic Ag_2S nanoparticles are observed (XRD: 6b; SEM: 6d), indicating that 150 ℃ is too low, or 17.5 h is too short for the as-prepared Ag_2S completely transforms to $AgInS_2$, which may be due to the strong adsorption properties of oleic acid. The oleic acid can be firmly adsorbed on the surface of as-prepared Ag_2S particles, which may hinder In^{3+} to replace the Ag^+, leading to the conversion rate to be greatly reduced, so it requires higher temperature or longer time to complete the transformation. This result shows that the solvent has a great influence on the phase and morphology of the products.

Table 2. Products Synthesized Using Other Solvents at 150 ℃ for 17.5 h

Sample	Solvent	XRD	Phase	SEM	Morphology
1	Ethylenediamine	Fig. 6a	Orthorhombic $AgInS_2$ + tetragonal $AgInS_2$ (minor)	Fig. 6c	Square nanoplate + particle (minor)
2	Oleic acid	Fig. 6b	Orthorhombic $AgInS_2$ + monoclinic Ag_2S	Fig. 6d	Particle

3. 5 UV-Vis diffuse reflectance spectroscopy

For I-III-VI family compounds, most of them are direct-narrow-gap semiconductors with chalcopyrite structure[23]. $AgInS_2$ has chalcopyrite and orthorhombic phases, and the band gap values are 1.87 and 1.98 eV, respectively[24-26]. Owing to its suitable bandgap, $AgInS_2$ has good absorption in the visible range, so it is a good photocatalytic material. Fig. 7 is the solid UV-Vis diffuse reflectance spectra of $AgInS_2$ nanoplates and $AgInS_2$ nanoparticles. The band gap of $AgInS_2$ can be calculated according to the formula (I)[4]:

$$\alpha h\nu = (h\nu - E_g)^{n} \qquad \text{(I)}$$

Here, α means the absorption coefficient; $h\nu$ is the photoelectron energy; the value of n is 1/2 for indirect bandgap compounds, while 2 for direct bandgap compounds, and E_g means the bandgap. Taking $h\nu$ as the abscissa, with $(\alpha h\nu)^{1/n}$ as ordinate, the curve is extended to intersect with the abscissa, and the bandgap can be calculated. As seen in Fig. 7a, the bandgap of $AgInS_2$ nanoplate is about 1.61 eV, close to the literature report of 1.58~1.63 eV[4, 12, 27]; while the bandgap of $AgInS_2$ nanoparticle is about 1.98 eV (Fig. 7b), consistent with the band gap of $AgInS_2$ crystal. The difference between the two gaps is probably caused by the different

particle sizes. Because the nanoplate has larger size (thickness about 40 nm, width 300～500 nm), while the nano particle is less than 20 nm, which results in the blue shift of the absorption edge due to small size effect.

3. 6 Photocatalytic activity of the $AgInS_2$ samples

The photocatalytic activities of $AgInS_2$ samples are measured on the degradation of methyl blue (MB) or methyl oragne (MO) in water under UV-Vis light irradiation. As shown in Fig. 8a, with the advance of illumination time, the absorbance of MB in solution is getting smaller and smaller, indicating that the concentration of MB is lower and lower. After 300 min of irradiation, the conversion of MB by $AgInS_2$ nanoparticles is about 66% (Fig. 8b, red curve). However, the conversion of MO by $AgInS_2$ nanoplates is about 25% (Fig. 8b, blue curve). The results show that $AgInS_2$ has certain ability on the photocatalytic degradation of organic dyes such as MB, and it is probably that the low-power tungsten halogen lamp (300 W) used in the experiment causes unexciting conversion. The possible mechanism on photocatalytic degradation of MB by $AgInS_2$ can be explained by the following equation[28]:

$$AgInS_2 + h\nu \leftrightarrow AgInS_2\,(h^+ + e^-) \qquad (6)$$

$$e^- + O_2 \rightarrow \bullet O_2^- \qquad (7)$$

$$2e^- + O_2 + 2H^+ \rightarrow H_2O_2 \qquad (8)$$

$$H_2O_2 + \bullet O_2^- \rightarrow OH^- + \bullet OH + O_2 \qquad (9)$$

$$\bullet OH/h^+/\bullet O_2^- + MB \rightarrow \text{intermediates} \rightarrow CO_2 + H_2O \qquad (10)$$

Scheme 2. Possible mechanism on photocatalytic degradation of MB by $AgInS_2$

Under UV-Vis light irradiation, the electrons transfer from valance band (VB) of $AgInS_2$ to the conduction band (CB), while the holes (h^+) generate in its VB (Reaction 6). The photogenerated electrons (e^-) can react with adsorbed O_2 to produce $\bullet O^{2-}$ (Reaction 7) and H_2O_2 (Reaction 8). H_2O_2 can further react with $\bullet O^{2-}$ and e^- to generate hydroxyl radicals ($\bullet OH$) (Reaction 9). All of $\bullet O_2^-$, h^+ and $\bullet OH$ play a role in the degradation and mineralization of MB (Reaction 10).

4 CONCLUSION

Two kinds of orthorhombic $AgInS_2$ nanostructures with different morphologies have been successfully prepared by the solvent method using KS_2CNR_2, $AgNO_3$, and $In(NO_3)_3$ as reagents. When using pyridine as the solvent, by tuning the reaction temperature and reaction time, it is found that pure $AgInS_2$ nanoplates with

relatively uniform morphology can be obtained at 120～150 ℃ for 17.5～20 h; when the temperature is below 120 ℃ or the reaction time is less than 10 h, most of the product is binary monoclinic Ag_2S, while there will be another ternary tetragonal $AgInS_2$ generated over 170 ℃. When using 1-dodecanethiol as the solvent, pure $AgInS_2$ nanoparticles with size less than 20 nm have been obtained at 120～190 ℃ for 17.5～20 h, indicating that the solvent has a great influence on the phase and morphology, and this point has also been verified using ethylenediamine or oleic acid as the solvent. On the other hand, UV-Vis diffuse reflectance spectra show that the bandgap of $AgInS_2$ nanoplates (1.61 eV) with larger size is less than that of $AgInS_2$ nanoparticles (1.98 eV) with smaller size, which is likely to be caused by the blue shift of absorption edge due to the small size effect. Furthermore, the photocatalytic experiments show that $AgInS_2$ has certain ability on photocatalytic degradation of organic dyes such as MB.

REFERENCES

(1) Ren, N. Q.; Guo, W. Q.; Zhou, X. J.; Yang, S. S. A review on treatment methods of dye wastewater. *J. Chem. Ind. Eng. (China)* **2013**, 64, 84–94.

(2) Zeng, Z.; Wang, A. Q.; Ping, L. L.; Yang, J. L.; Wang, Q. M. Encapsulation of lanthanides in ternary Ⅰ-Ⅲ-Ⅵ $AgInS_2$ nanocrystals and their physical properties. *Mater. Lett.* **2015**, 141, 225–227.

(3) Peng, S. J.; Zhang, S. J.; Mhaisalkar, S. G.; Ramakrishna, S. Synthesis of $AgInS_2$ nanocrystal ink and its photoelectrical application. *Phys. Chem. Chem. Phys.* **2012**, 14, 8523–8529.

(4) Zou, X. J.; Dong, Y. Y.; Rang, C. Q.; Cui, Y. B.; Chen, Z. B. Fabrication of flower-like $AgInS_2$ microsphere and its photocatalytic reduction of Cr(Ⅵ). *J. Wuhan Univ. (Nat. Sci. Ed.)* **2016**, 62, 92–96.

(5) Bu, C. F.; Liu, L. W.; Wang, Q.; Zhang, B. T.; Hu, S. Y.; Ren, Y.; Zhu, L. X. Folic acid-conjugated $AgInS_2$ quantum dots for in vitro cancer cell imaging. *Chin. J. Lumin.* **2015**, 36, 989–995.

(6) Chevallier, T.; Blevennec, G. L.; Chandezonb, F. Photoluminescence properties of $AgInS_2$-ZnS nanocrystals: the critical role of the surface. *Nanoscale* **2016**, 8, 7612–7620.

(7) Azam, E. S. Photocatalytic oxidation of cyanide under visible light by Pt doped $AgInS_2$ nanoparticles. *J. Ind. Eng. Chem.* **2014**, 20, 4008–4013.

(8) Cai, C. Q.; Zhai, L. L.; Ma, Y. H.; Zou, C.; Zhang, L. J.; Yang, Y.; Huang, S. M. Synthesis of $AgInS_2$ quantum dots with tunable photoluminescence for sensitized solar cells. *J. Power Sources* **2017**, 341, 11–18.

(9) Wang, L.; Kang, X. J.; Pan, D. C. Gram-scale synthesis of hydrophilic PEI-coated $AgInS_2$ quantum dots and its application in hydrogen peroxide/glucose detection and cell imaging. *Inorg. Chem.* **2017**, 56, 6122–6130.

(10) Yoshino, K.; Komaki, H.; Kakeno, T.; Akaki, Y.; Ikari, T. Growth and characterization of *p*-type $AgInS_2$ crystals. *J. Phys. Chem. Solids* **2003**, 64, 1839–1842.

(11) You, S. H.; Hong, K. J.; Lee, B. J.; Jeong, T. S.; Youn, C. J.; Park, J. S.; Baek, S. N. Temperature dependence of band gap and photocurrent properties for the $AgInS_2$ epilayers grown by hot wall epitaxy. *J. Cryst. Growth* **2002**, 245, 261–266.

(12) Wei, Q. L.; Zhao, X. L.; Yao, P. P.; Mu, J. Preparation and visible light photocatalytic activity of $AgInS_2$ nanoparticles. *Chin. J. Inorg. Chem.* **2011**, 27, 692–694.

(13) Kharkwal, A.; Nitu, K.; Jain, S. B.; Tyagi, S. B.; Kharkwal, M. Novel synthesis of selective phase-shape orientation of $AgInS_2$ nanoparticles at low temperature. *Colloid Polym. Sci.* **2015**, 293, 1953–1959.

(14) Hong, S. P.; Park, H. K.; Oh, J. H.; Yang, H.; Do, Y. R. Comparisons of the structural and optical properties of o-$AgInS_2$, t-$AgInS_2$ and c-$AgIn_5S_8$ nanocrystals and their solid-solution nanocrystals with ZnS. *J. Mater. Chem.* **2012**, 22, 18939–18949.

(15) Torimoto, T.; Adachi, T.; Okazaki, K. Facile synthesis of ZnS-$AgInS_2$ solid solution nanoparticles for a color-adjustable luminophore. *J. Am. Chem. Soc.* **2007**, 129, 12388–12389.

(16) Wang, Y.; Zou, X. C.; Wang, C.; Shi, Y. F. Thermolysis synthesis and growth mechanism of metastable $MInS_2$ (M = Ag, Cu) flowerlike microsphere. *Chin. J. Inorg. Chem.* **2016**, 32, 2151–2157.

(17) Liu, Z. P.; Tang, K. B.; Wang, D. K.; Wang, L. L.; Hao, Q. Y. Facile synthesis of $AgInS_2$ hierarchical flowerlike nanoarchitectures composed of ultrathin nanowires. *Nanoscale* **2013**, 5, 1570–1575.

(18) Zou, Z. G.; Gap, Y.; Long, F.; Zhang J. Synthesis and mechanism of Wurtzite $CuInS_2$ nanocrystals. *J. Synth. Cryst.* **2015**, 44, 2164–2170.

(19) Shi, Y. F.; Wang, Y.; Wu, L. M. Hexagonal MIn_2S_4 (M = Mn, Fe, Co): formation and phase transition. *J. Phys. Chem. C* **2013**, 117, 20054–20059.

(20) Fang, F.; Chen, L.; Chen, Y. B.; Wu, L. M. Syntheses and photocatalysis of $ZnIn_2S_4$ nano/micropeony. *J. Phys. Chem. C* **2010**, 114, 2393–2397.

(21) Lu, X.; Zhuang, Z.; Peng, Q.; Li, Y. Controlled synthesis of wurtzite $CuInS_2$ nanocrystals and their side-by-side nanorod assemblies. *CrystEngComm.* **2011**, 13, 4039–4045.

(22) Delgado, G.; Mora, A. J.; Pineda, C.; Tinoco, T. Simultaneous Rietveld refinement of three phases in the Ag-In-S semiconducting system from X-ray powder diffraction. *Mater. Res. Bull.* **2001**, 36, 2507–2517.

(23) Xie, C. P.; Xiang, W. D.; Luo, L.; Zhong, J. S.; Zhao, B. Y.; Liang, X. J. Advances on $AgInS_2$ quantum dots. *J. Funct. Mater.* **2014**, 45, 4009–4016.

(24) Hu, J. Q.; Lu, Q. Y.; Tang, K. B.; Qian, Y. T.; Hu, J. Q.; Lu, Q. Y.; Tang, K. B.; Qian, Y. T.; Zhou, G. E.; Liu, X. M. Solvothermal reaction route to nanocrystalline semiconductors $AgMS_2$ (M = Ga, In). *Chem. Commun.* **1999**, 12, 1093–1094.

(25) Aguilera, M. L. A.; Hernandez, J. R. A.; Trujillo, M. A. G.; Lopez, M. O.; Puente, G. C. Photoluminescence studies of chalcopyrite and orthorhombic $AgInS_2$ thin films deposited by spray pyrolysis technique. *Thin Solid Films* **2007**, 515, 6272–6275.

(26) Aguilera, M. L. A.; Ortega-Lopez, M.; Resendiz, V. M. S.; Hernández, J. A.; Trujillo, M. A. G. Some physical properties of chalcopyrite and orthorhombic $AgInS_2$ thin films prepared by spray pyrolysis. *Mater. Sci. Eng. B* **2003**, 102, 380–384.

(27) Li, X. M.; Niu, J. Z.; Shen, H. B.; Xu, W. W.; Wang, H. Z.; Li, L. S. Shape controlled synthesis of tadpole-like and heliotrope seed-like *$AgInS_2$* nanocrystals. *Cryst. Eng. Comm.* **2010**, 12, 4410–4415.

(28) Deng, F.; Zhong, F.; Hu, P.; Pei, X. L.; Luo X. B.; Luo, S. L. Fabrication of In-rich $AgInS_2$ nanoplates and nanotubes by a facile low-temperature co-precipitation strategy and their excellent visible-light photocatalytic mineralization performance. *J. Nanopart. Res.* **2017**, 19, 14.

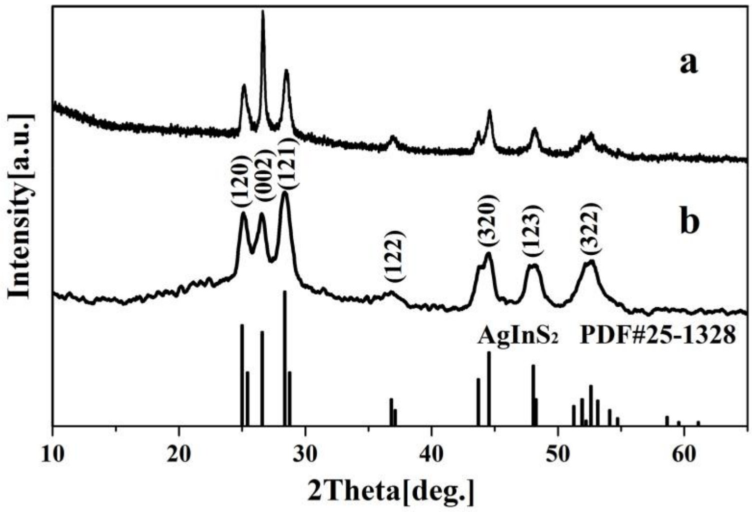

Fig. 1. XRD pattern of the as-prepared $AgInS_2$ samples:

(a) 120 ℃/20 h, pyridine as the solvent; (b) 150 ℃/17.5 h, 1-dodecanethiol as the solvent

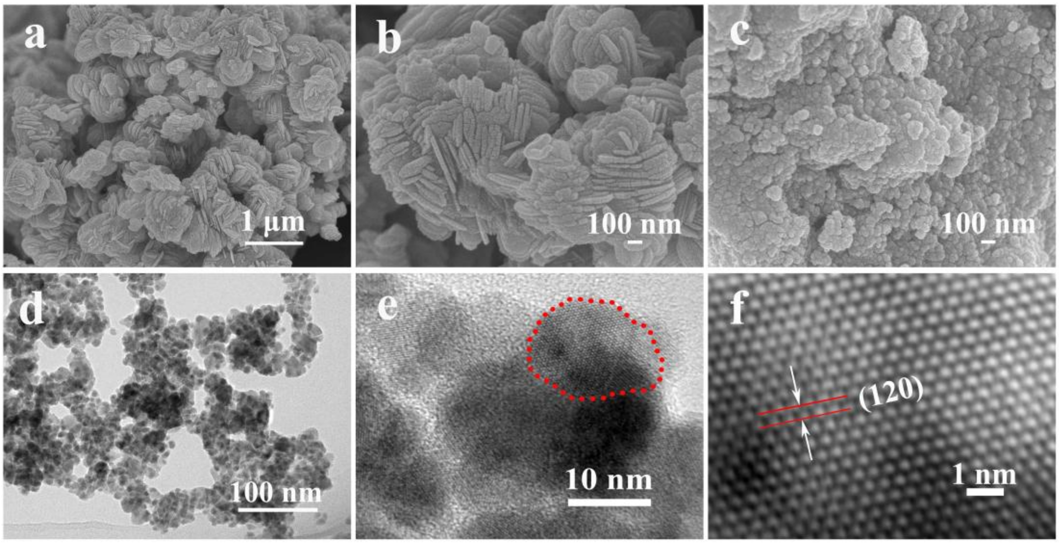

Fig. 2. (a, b) SEM images of $AgInS_2$ samples prepared at 120 ℃ for 20 h, using pyridine as the solvent; (c, d) SEM and TEM images of $AgInS_2$ samples prepared at 150 ℃ for 17.5 h, using 1-dodecanethiol as the solvent; (e, f) HRTEM images of particle in picture d, indicating that the size of that particle is about 14 nm (calculated by the red circle), and the interplanar spacing is 0.357 nm, in good agreement with the distance (0.356 nm) of (120) planes of orthorhombic $AgInS_2$

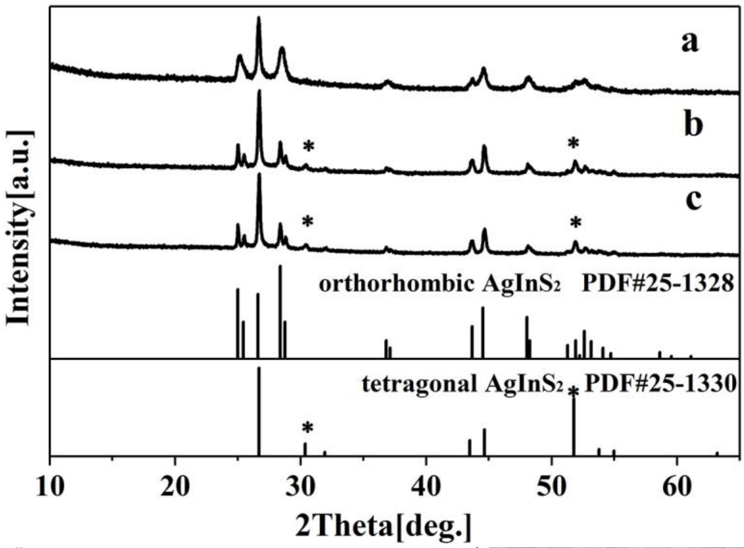

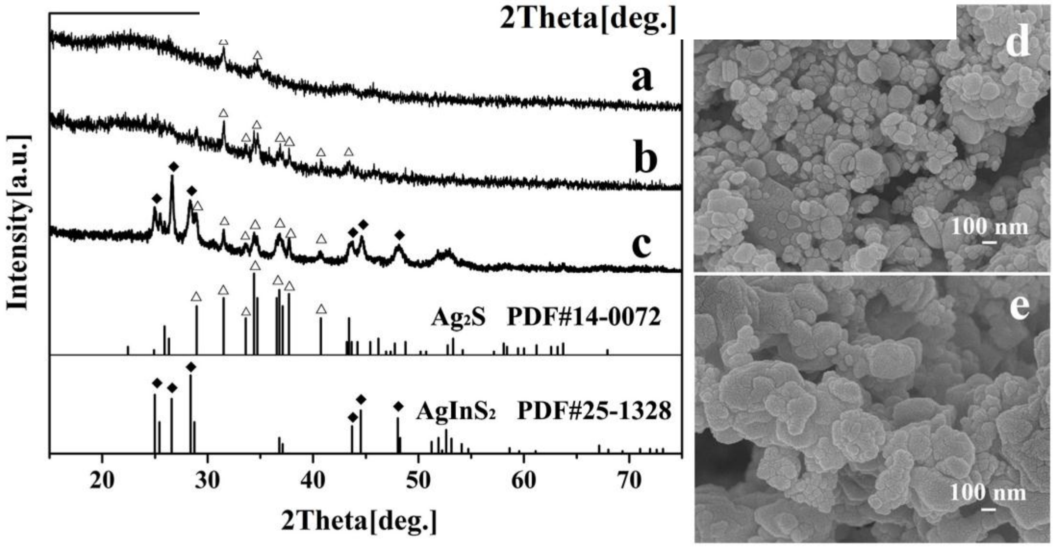

Fig. 3. XRD patterns and SEM images of products prepared at 120 ℃ for different time: (a) 5 h, weak diffraction peak, monoclinic Ag_2S; (b, d) 10 h, monoclinic Ag_2S, similar quantity of nanoplate and nanoparticle; (c, e) 15 h, the major orthorhombic $AgInS_2$ with minor monoclinic Ag_2S, and the quantity of nanoplate is much larger than nanoparticle

Fig. 4. XRD patterns of products prepared at different temperature for 17.5 h using pyridine as the solvent: (a) 150 ℃, orthorhombic $AgInS_2$; (b) 170 ℃, orthorhombic $AgInS_2$ (major) + tetragonal $AgInS_2$ (minor); (c) 190 ℃, orthorhombic $AgInS_2$ (major) + tetragonal $AgInS_2$ (minor)

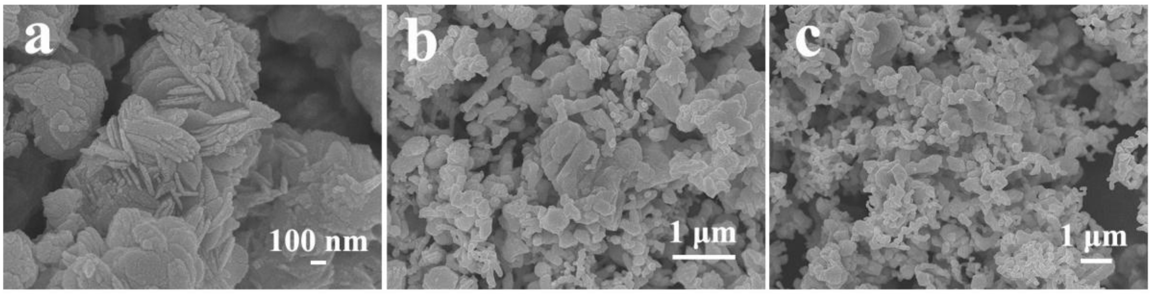

Fig. 5. TEM images of products prepared at different temperature for 17.5 h using pyridine as the solvent: (a) 150 ℃; (b) 170 ℃; (c) 190 ℃

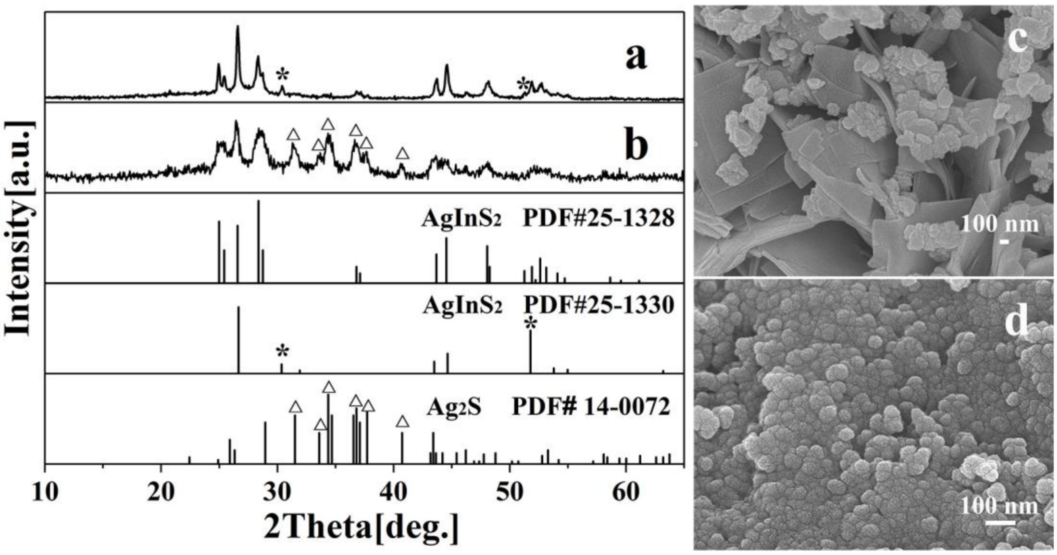

Fig. 6. XRD patterns and SEM images of products prepared at 150 ℃ for 17.5 h using other solvents: (a, c) ethylenediamine, orthorhombic $AgInS_2$ + tetragonal $AgInS_2$ (minor), square nanoplate + particle (minor); (b, d) oleic acid, orthorhombic $AgInS_2$ + monoclinic Ag_2S, nanoparticle

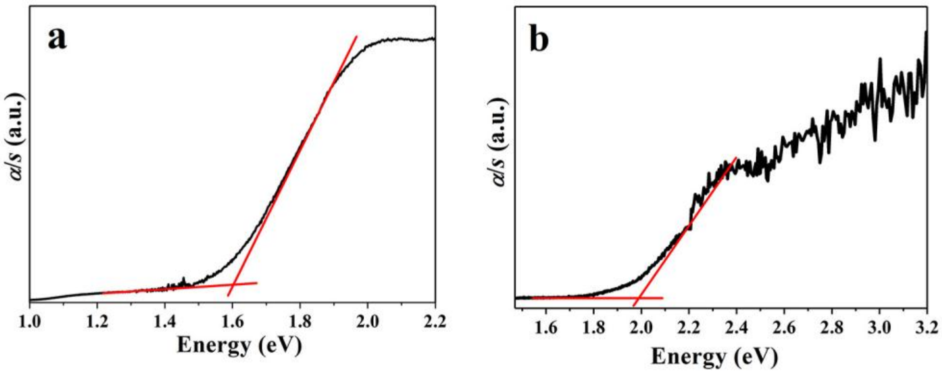

Fig. 7. UV-Vis diffuse reflectance spectrum of as-prepared products: (a) $AgInS_2$ nanoplate, synthesized at 120 ℃ for 20 h using pyridine as the solvent. The bandgap is about 1.61 eV; (b) $AgInS_2$ nanoparticle, synthesized at 150 ℃ for 17.5 h using 1-dodecanethiol as the solvent. The bandgap is about 1.98 eV

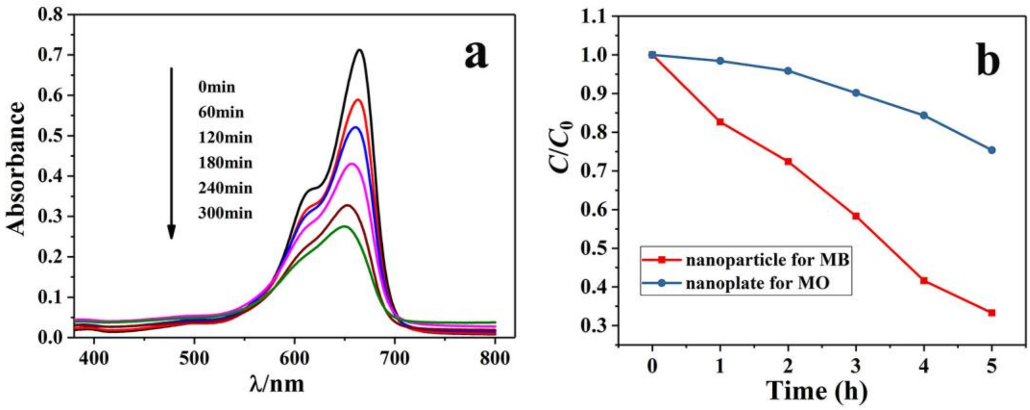

Fig. 8. (a) Absorption spectra of MB photocatalytic degraded by $AgInS_2$ nanoparticle; (b) Relation between MB concentration and time photocatalytic degraded by $AgInS_2$ nanoparticle (the red curve), and the relation between MO concentration and time photocatalytic degraded by $AgInS_2$ nanoplate (the blue curve)

Solvent Synthesis, Growth Mechanism and Photocatalytic Properties of $AgInS_2$ Nanoplate and Nanoparticle

WANG Yue(王 跃) SHI Yong-Fang(石永芳) LI Xiao-Bo(李晓波)

LI Dong-Wei(黎东维) ZHANG Tao(张涛) HE Yu-Cen(何昱岑)

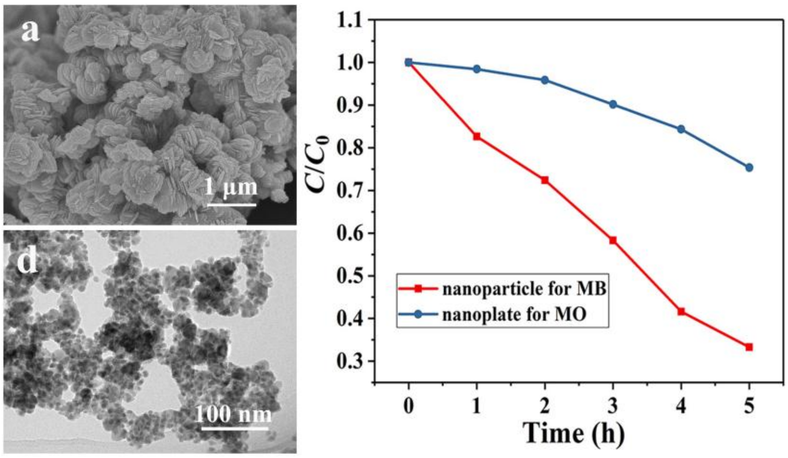

$AgInS_2$ nanoplate and nanoparticle were synthesized using pyridine and 1-dodecanethiol as the solvents. The reaction temperature, reaction time and solvent have an influence on the phase and morphology of $AgInS_2$, and both $AgInS_2$ nanoplate and nanoparticle have some ability on the photocatalytic degradation of organic dyes under UV-Vis light irradiation.